

Simulation of the tensile failure behaviour of transversally bedding layers using PFC2D

Hadi Haeri^{*1}, Vahab Sarfarazi^{2a}, Zheming Zhu^{**1} and Mohammad Fatehi Marji^{3b}

¹College of Architecture and Environment, Sichuan University, Chengdu 610065, China

²Department of Mining Engineering, Hamedan University of Technology, Hamedan, Iran

³Department of Mining Engineering, Yazd University, Yazd, Iran

(Received March 30, 2018, Revised June 2, 2018, Accepted June 7, 2018)

Abstract. In this paper, the tensile failure behaviour of transversally bedding layers was numerically simulated by using particle flow code in two dimensions. Firstly, numerical model was calibrated by uniaxial, Brazilian and triaxial experimental results to ensure the conformity of the simulated numerical model's response. Secondly, 21 circular models with diameter of 54 mm were built. Each model contains two transversely bedding layers. The first bedding layer has low mechanical properties, less than mechanical properties of intact material, and second bedding layer has high mechanical properties, more than mechanical properties of intact material. The angle of first bedding layer, with weak mechanical properties, related to loading direction was 0°, 15°, 30°, 45°, 60°, 75° and 90° while the angle of second layer, with high mechanical properties, related to loading direction was 90°, 105°, 120°, 135°, 150°, 160° and 180°. It is to be noted that the angle between bedding layer was 90° in all bedding configurations. Also, three different pairs of the thickness were chosen in models; i.e., 5 mm/10 mm, 10 mm/10 mm and 20 mm/10 mm. The result shows that in all configurations, shear cracks develop between the weaker bedding layers. Shear cracks angle related to normal load change from 0° to 90° with increment of 15°. Numbers of shear cracks are constant by increasing the bedding thickness. It is to be noted that in some configuration, tensile cracks develop through the intact area of material model. There is not any failure in direction of bedding plane interface with higher strength.

Keywords: bedding layer; intersection; Brazilian tensile strength; PFC2D

1. Introduction

A nearly homogeneous concrete structure can be changed into a highly heterogeneous one due to the existence of some intrinsic discontinuities such as fractures, joints, and cracks. The mechanical behavior of the heterogeneous material is highly changed and controlled by these discontinuities which render the material as anisotropic too (Amadei 1996, Jiang *et al.* 2006, Fortsakis *et al.* 2012, Xu *et al.* 2013, Yu *et al.* 2014, Wasantha *et al.* 2015, Li *et al.* 2016, Johansson 2016).

In general, the tensile strengths of concretes are much lower than their shear and compressive strengths due to some planes of weaknesses which can be induced within the concrete during the relatively lower level of applied tensile loading. These weak planes can significantly contribute to the anisotropic behaviours of concrete. Therefore, anisotropy of jointed concrete under tensile loading condition is a very important task and can be explored in the field of geomechanical engineering. Therefore, the standard indirect tensile tests (Brazilian tensile tests) of

concrete discs have gained a wide application and widely conducted in the concrete and rock mechanics laboratories to study the tensile behaviours of concrete materials (Vervoort *et al.* 2014, Dan and Konietzky 2014, Duan and Kwok 2015, Wang *et al.* 2016a, b, c, Khosravi *et al.* 2017, Xia *et al.* 2017, Yuan and Shen 2017, Zhang *et al.* 2018). It has been observed that anisotropy can highly change the indirect tensile strength of the laminated (stratified) concretes specimens. The tensile strength of anisotropic laminated concrete samples can be determined by using the standard Brazilian tensile tests (Wu *et al.* 2010, Cho *et al.* 2012, Liu *et al.* 2013, Dan *et al.* 2013, Tavallali and Vervoort 2010, Khanlari *et al.* 2015).

However, it has been concluded that as a whole, the tensile strength of concrete is apparently affected by its anisotropy. It has been observed that the concrete specimens have failed along the loaded diameter of the discs irrespective of the orientation of joint planes. The failed anisotropic concrete specimens contain cracks that their total lengths vary and have certain relationships with the joints inclination angles. Two major modes of failure were found for fractured concrete specimens by Khanlari *et al.* (2015). They observed that in the laminated concrete (rock) specimens, the fractures usually occur parallel to the loading direction with or without branching at inclination angles lower than 60°. For the inclination angles greater than 60° the fractures occur in the direction of lamination so that a failure mode along the laminations dominates. The effect of anisotropy on the tensile strength of concrete (rock) has been studied by Ma *et al.* (2017a, b). They

*Corresponding author, Professor

E-mail: haerihadi@gmail.com

**Corresponding author, Professor

E-mail: zhemingzhu@hotmail.com

^aAssistant Professor

^bAssociate Professor

considered that the anisotropy ratio and tensile strength have a great influence on the fracture (failure) stress. The influence of anisotropy on the fracture stress of rocks (layered shale samples) has been emphasized. By Zhang *et al.* (2018) who studied the fracture patterns of the layered shale Brazilian discs under indirect tensile testing condition using the acoustic emission (AE) technique. The spatial distribution of AE related to the bedding angles was investigated which resulted in a better understanding of the mechanism of anisotropic failure process in the layered rocks. The fracture network system may also play a significant role in the compressive and shear strengths of many rock masses as investigated by many researches and reported in the concrete and rock mechanics literature (Min and Jing 2003, Jia and Tang 2008, Wang *et al.* 2012, Zhou and Yang 2012, Lancaster *et al.* 2013, Mobasher *et al.* 2014, Noel and Soudki 2014, Oliveira and Leonel 2014, Kim and Taha 2014, Tiang *et al.* 2015, Wan Ibrahim *et al.* 2015, Silva *et al.* 2015, Gerges *et al.* 2015, Liu *et al.* 2015, Haeri 2015, Haeri *et al.* 2015a, b, Haeri *et al.* 2016, Zhou and Wang 2016, Shemirani *et al.* 2016, Fan *et al.* 2016, Li *et al.* 2016, Sardemir 2016, Sarfarazi *et al.* 2016, Shuraim 2016, Wang *et al.* 2016a, b, c, Yang *et al.* 2017, Wang *et al.* 2017, Sarfarazi *et al.* 2017a, b, c, Wang *et al.* 2017, Zhou *et al.* 2018, Bahaaddini *et al.* 2014, Bahaaddini *et al.* 2016a, b, Shemirani *et al.* 2018, Zhou and Bi 2018, Haeri *et al.* 2013, Haeri *et al.* 2014, Haeri 2015, Haeri and Sarfarazi, 2016a, b, Haeri *et al.* 2016a, b).

However, rare results have been reported regarding the effect of anisotropy induced by the presence of complex discontinuities on the tensile strength of brittle rocks and concretes. Typical fracture pattern and failure process have been found for an underground excavation resulting from the presence of natural joints by Li (2013) and some tensile fractures were observed in the in-situ surveyed area. A strong anisotropic condition was observed by Lisjak *et al.* (2015) for a tunnel cross-section while measuring its average convergence.

The displacements in a perpendicular direction to the bedding planes orientation are approximately four times higher than those measured parallel to the bedding. It has been observed that the deformation in the stratified Lias limestone (Seingre 2005) in Löttschberg tunnel are high enough to deform the steel sets and surrounding concrete used as support system. These deformations were greatly influenced by the orientation of the rock mass discontinuities. Many numerical analyses have shown that the deformed shape of the tunnel cross-section considering the rock anisotropy is always perpendicular to the direction of discontinuities in the transversely isotropic laminated rocks and concretes (Jia and Tang 2008, Fortsakis *et al.* 2012, Wang *et al.* 2012). It has been shown that when considering the anisotropy in rocks and concretes the displacement is always perpendicular to the discontinuities direction for the transversely isotropic structures. This result is in very good agreement with the deformations observed in the real case studies related to tunnel and underground excavation (Seingre 2005, Li 2013, Lisjak *et al.* 2015, Yang *et al.* 2015). It means that studying the anisotropy of the jointed concrete can be used as a key element to consider its influence of the development of deflections and deformations in the in situ stratified rocks. Therefore, many researchers have tried to accomplish some experimental

tests on the transversely isotropic concretes samples (Lazear 2009, Cho *et al.* 2012, Gholami and Rasouli 2014, Dan and Konietzky 2014, Vervoort *et al.* 2014, Duan and Kwok 2015).

In this research, it has been tried to investigate numerically the effects of bedding layers and their imposed anisotropy on the tensile strength of concrete using a sophisticated discrete element approach implemented in a two dimensional particle flow code (PFC2D). PFC 2D can simulate the failure behavior of transversally bedding layer where other software are disable.

2. Numerical modeling with particle flow code (PFC)

Any PFC2D software supports two basic bonding models i.e., a contact-bonded model and a parallel-bonded model. The concrete materials are simulated using the bonded particle modelling approach adopted in PFC2D. In this modelling approach, each concrete specimen is considered as a circular discs assembly bonded together at some specified contact points and confined by the planar walls. The competence of concrete is simulated by the bonded particles which are bonded together at their contacts points. The physical behavior of a vanishingly small cement-like substance lying in between the particles and joining the two bonded particles is approximated by a contact bond modelling approach. On the other hand, in a parallel bond modelling approach each contact bond model behaves as a parallel bond of radius zero. Therefore, a contact bond does not have a radius and the shear and normal stiffnesses are also zero, like a parallel bond. Any contact bond model cannot resist a bending moment but it can only resist forces acting at the contact points. However, the contacts bonds are usually assigned with specified tensile and shear strengths which allows the material resistance to tension and shear which may exist at the contacts points until the contact force at these points exceeds the strength of the bonds (Itasca 1999, Potyondy 2004).

A contact-bonded particle model can be generated for PFC2D by providing the routines given rence (25). The following micro parameters should be defined for applying a contact bond model i.e., i) a proper modulus for each ball-to-ball contact, ii) a proper stiffness ratio k_n over k_s , for the frictional coefficient of the balls, iii) the normal bond strength of the contact points, vi) the shear bond strength of the contacts, v) the ratio of standard deviation to mean of bond strength both in normal and shear directions, and vi) the minimum ball (circle) radius. Where as to define a parallel-bonded particle model requires three additional micro parameters i.e., i) the parallel-bond radius multiplier, ii) the parallel-bond modulus, and iii) the stiffness ratio of the parallel-bond.

In the present research, the parallel bonding of the particles can also be used as the bonded particle models assuming that the assembly of particles are joined and bonded together.

For the establishment of the parallel bonded modelling approach the appropriate micro parameters should be

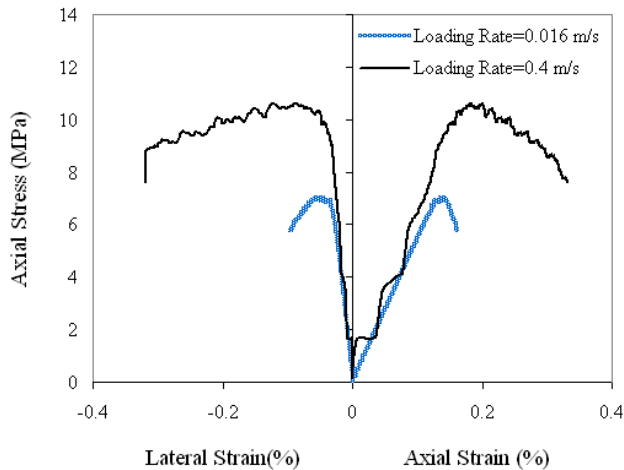


Fig. 1 The effect of the loading rate on the: (a) curve of axial stress versus axial strain

selected for the particle assembly by conducting a calibration procedure.

However, it is not reasonable to directly use the experimental testing laboratory results for the numerically used parameters which govern the particles contact properties and their bonding characteristics. Laboratory testing results give the macro-mechanical properties of the materials which are reflected due to their continuum behaviour. Therefore, the appropriate micro-mechanical properties of the bonded particles can be determined using an inverse modelling procedure and laboratory testing results. The trial and error approach is a proper method for the calibration of these micromechanical parameters since no direct theory exists relating these two sets of material property (Potyondy 2004). This procedure assumes the reasonable micro-mechanical parameter values for the particles and then a comparison of the strength and deformation characteristics of the numerical models to those of the laboratory samples are being made to adjust these parameters. This procedure is repeated so that adjusted micro-mechanical property values which give better simulated macroscopic responses that are very close to those of the laboratory testing results can be gained for the jointed blocks of a rock mass.

2.1 Preparing and calibrating the numerical model

The standard procedure of particle assembly generation is used by PFC2D software. (Itasca 1999). This particles generating process involves the following five basic steps: i) the geometrical particle generation, ii) the packing of the particles, iii) the isotropic stress installation (stress initialization), iv) the elimination of floating particle (floaters) and v) the installation of bonds. However, the gravity effect is not taking into account as the modelled specimen is small and the gravity-induced stress gradient has negligible effect on the macroscopic behavior of the specimen.

The three standard tests which are: i) the unconfined compressive strength test, ii) the Brazilian tensile test and iii) the biaxial compressive test are being carried out in a

Table 1 Micro properties used to represent intact concrete

Parameters	Values	Parameters	Values
Type of particles	Disc	Parallel-bond radius multiplier	1
Density (kg/m ³)	1000	Young's modulus of parallel bond (GPa)	4
Minimum radius (mm)	0.27	Parallel bond stiffness ratio	1.7
Size ratio	1.56	Particle friction coefficient	0.4
porosity	0.08	Parallel bond normal strength, mean (MPa)	5.6
Damping ratio	0.7	Parallel bond normal strength, std. dev. (MPa)	1.4
Contact Young's modulus (GPa)	4	Parallel bond shear strength, mean (MPa)	5.6
Stiffness ratio	1.7	Parallel bond shear strength, std. dev. (MPa)	1.4

rock mechanics laboratory to calibrate the properties of particles and parallel bonds in bonded particle model. A sufficiently small applied loading rate is used in each test to ensure that the force, displacement, velocity and acceleration of any particle within the assembly cannot propagate farther than its immediate neighbours during a single time step. This low loading rate also cause that the loaded sample remains in quasi-static equilibrium throughout the test

Effect of loading rate on the axial stress strain curve is shown in Fig. 1. The testing samples are being modelled by 14298 particles and their mechanical responses clearly depend on the loading rate in the elastic region of the stress strain curve. If the loading rate increases to that of 0.4 m/s, an oscillatory behaviour in the stress-strain curve is produced. However, this oscillatory behaviour of the mechanical response is greatly reduced at smaller loading rates (i.e., 0.016 m/s for the curve shown in Fig. 1).

Based on the above explanation, a proper loading rate of 0.016 m/s is adopted for the PFC2D simulated tests in this study. Then, using the micro-properties listed in Table 1 and the standard calibration procedures (Potyondy 2004), a calibrated PFC particle assembly was created. The specifications of different numerical tests for model calibration are summarized in following section.

2.1.1 Numerical unconfined compressive test

The unconfined (uniaxial) compression test in PFC2D can be modelled by considering two moving walls compressing the particles assembly, as illustrated in Fig. 2(a). The solid lines indicate the bonds break where the micro-cracks can be induced and cause the samples failure. The black line represents the tensile failure and the red one indicated the shear failure. The frictionless rigid plates are taken as the walls of the modelled specimen. The specimen's assembly is 108 mm in height, 54 mm in width and consists of 14298 particles. The particle size distribution is taken to be normal with particle radii ranging from 0.27 mm to 0.4212 mm. The bounds of these small particles radii are chosen so that these particles dimensions are kept as small as possible, without increasing the computational efficiency of PFC2D, and also minimizing its total running time. A reasonable value for the porosity ratio is obtained (i.e., 0.08), which produces a dense Packing specimen. However, the elastic modulus (E), Poisson's

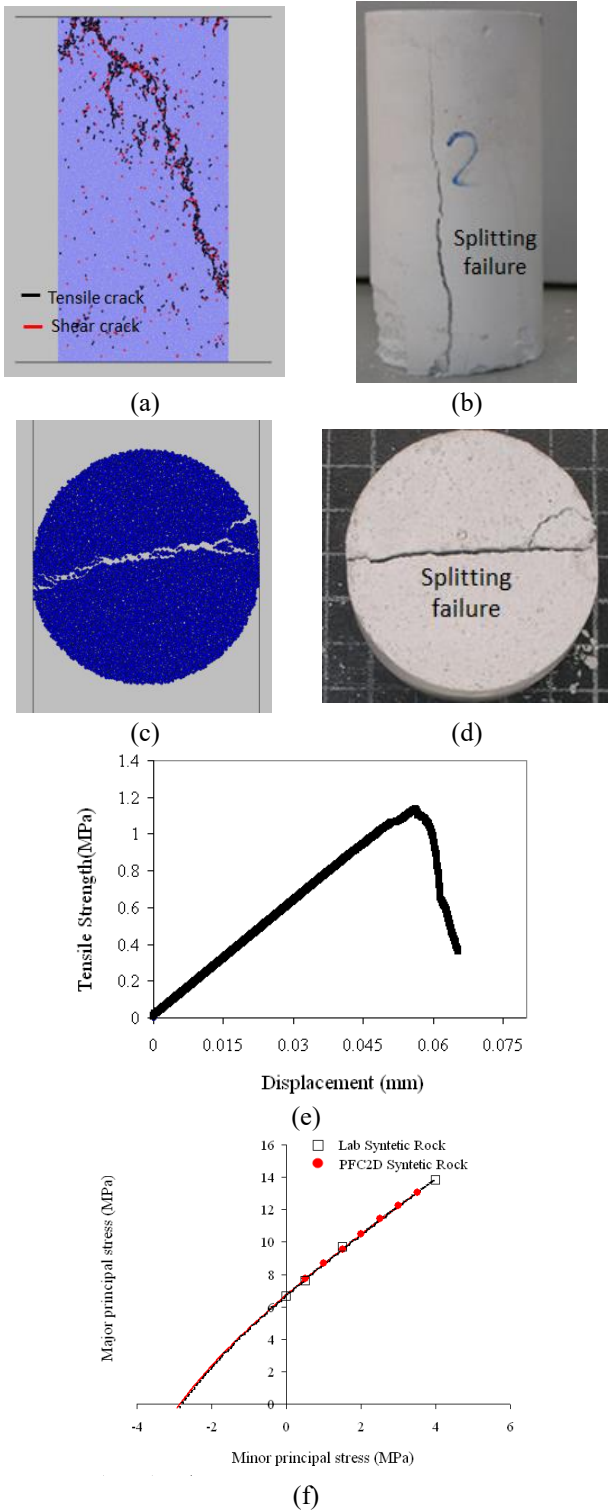


Fig. 2(a) Unconfined compressive test (cracks described by red/black lines), (b) failure pattern in physical uniaxial sample, (c) failure pattern in PFC2D model, (d) failure pattern in physical sample, (e) Tensile strength versus axial displacement curve for numerical Brazilian test simulation, (f) Calibrated failure locus for PFC synthetic concrete compared to the Laboratory measured

ratio, crack initiation stress and unconfined compression strength (UCS) of the particle assembly can be obtained by

Table 2 Macro mechanical properties of model material in experimental test and PFC2D

Mechanical Properties	Experimental results	PFC2D Model results
Elastic modulus, (GPa)	5	5
Poisson's ration	0.18	0.19
UCS, (MPa)	6.6	6.7
Crack initiation stress (MPa)	3.2	3.2
Brazilian tensile strength _t (MPa)	1	1.1
Friction angle	20.4	21
Cohesion (MPa)	2.2	2.2

Table 3 micro properties of low and high strength of bedding layer interfaces

Parameter	Low Value	High value	Parameter	Low value	High value
n_bond	1e3	1e6	s_bond	1e3	1e6
fric	0.25	0.5			

this simulation procedure. A basically vertical failure plane is achieved which is in agreement with experimental observation of the Laboratory tested specimens as shown in Fig. 2. A comparison of the mechanical properties obtained experimentally and numerically are presented in Table 2.

2.1.2 Brazilian test

Brazilian test was used to calibrate the tensile strength of the specimen in PFC2D model. The diameter of the Brazilian disk used in the numerical tests is 54 mm in diameter, and is made of 5615 particles. The disk was crushed by the lateral walls moved towards each other with a low speed of 0.016 m/s. Figs. 2(c) and (d) show failure patterns in both of the PFC2D numerical model and experimental sample; respectively. The splitting plane is basically horizontal and it agrees well with the experimental observation. Fig. 2(e) shows the tensile strength versus the axial displacement curve for PFC2D numerical brazilian simulation. From Fig. 8(e), it's clear that the bonded particles have a brittle behavior under indirect tensile loading so that they have reached their peak tensile strength and got broken before they get into non-linear deformation stage. The Numerical tensile strength with the comparison of the experimental measurements is presented in Table 2.

2.1.3 Biaxial test

The specifications of tested specimen in biaxial test are the same as that in uniaxial test. For biaxial testing, the rectangle model is loaded by surrounding four walls so that the top and bottom walls serve as loading platens, while the side walls serve to maintain a specified confining stress. The lateral wall normal stiffnesses are set equal to a fraction (0.001-0.2) of the average particle normal stiffness to simulate a soft confinement. The confined and vertical stresses are applied to the specimen by activating the servo-mechanism that controls the velocities of the four confining walls. Fig. 2(f) gives the strength envelope for the synthetic material and the PFC strength. It shows that the PFC2D predicts the biaxial behaviour of the numerical model

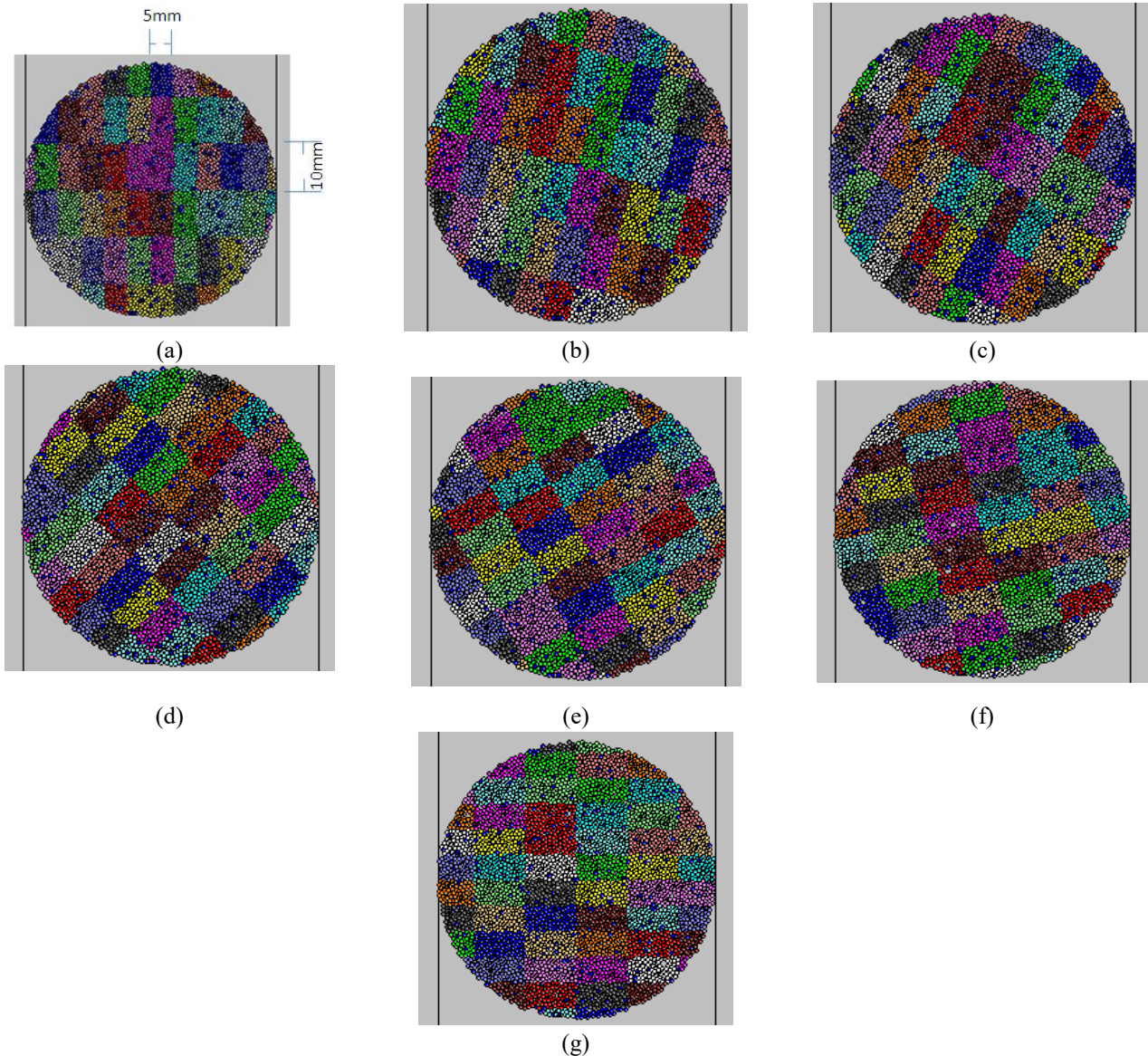


Fig. 3 The models with bedding layers thicknesses of 5 mm and 10 mm; bedding layers angle are (a) 0° - 90° , (b) 15° - 105° , (c) 30° - 120° , (d) 45° - 135° , (e) 60° - 150° , (f) 75° - 165° , (g) 90° - 180°

according to the experimental one. The Numerical shear properties with the comparison of the experimental measurements are presented in Table 3. As the numerical results agreed with experimental measurements, it was concluded that the assembly constructed in PFC2D could realistically represent for the mechanical behaviour of a concrete like material. Therefore, the parameters used for the above numerical tests, which was listed in Table 2, could be introduced in the subsequent modelling of shear behaviour of non-persistent joint.

2.2 Numerical uniaxial test on the non-persistent open joint

2.2.1 Preparing the model

After calibration of PFC2D, brazilian tests on transverse bedding layers were numerically simulated by creating a circular model in PFC2D (by using the calibrated micro parameters) (Figs. 3, 4 and 5). The PFC specimen has the

cross sectional diameter of 54 mm. A total of 81179 disks with a minimum radius of 0.27 mm were used to make up the specimen. The particles are surrounded by two loading walls. Transversely bedding layers consisted of two unparallel bedding layers. The angle of first bedding layer, with weak mechanical properties, related to loading direction was 0° (Fig. 3(a)), 15° (Fig. 3(b)), 30° (Fig. 3(c)), 45° (Fig. 3(d)), 60° (Fig. 3(e)), 75° (Fig. 3(f)) and 90° (Fig. 3(g)) while the angle of second layer, with high mechanical properties, related to loading direction was 90° (Fig. 3(a)), 105° (Fig. 3(b)), 120° (Fig. 3(c)), 135° (Fig. 3(d)), 150° (Fig. 3(e)), 165° (Fig. 3(f)) and 180° (Fig. 3(g)). Is to be note that the angle between bedding layer was 90° in all bedding configurations. Also, three different pairs of the thickness was chosen in models; i.e., 5 mm/10 mm (Fig. 3), 10 mm/10 mm (Fig. 4), and 20 mm/10 mm (Fig. 5). The disk was crushed by lateral walls, moving towards each other with a low speed of 0.016 m/s. Micro-properties of two different bedding layer interfaces were chosen too low

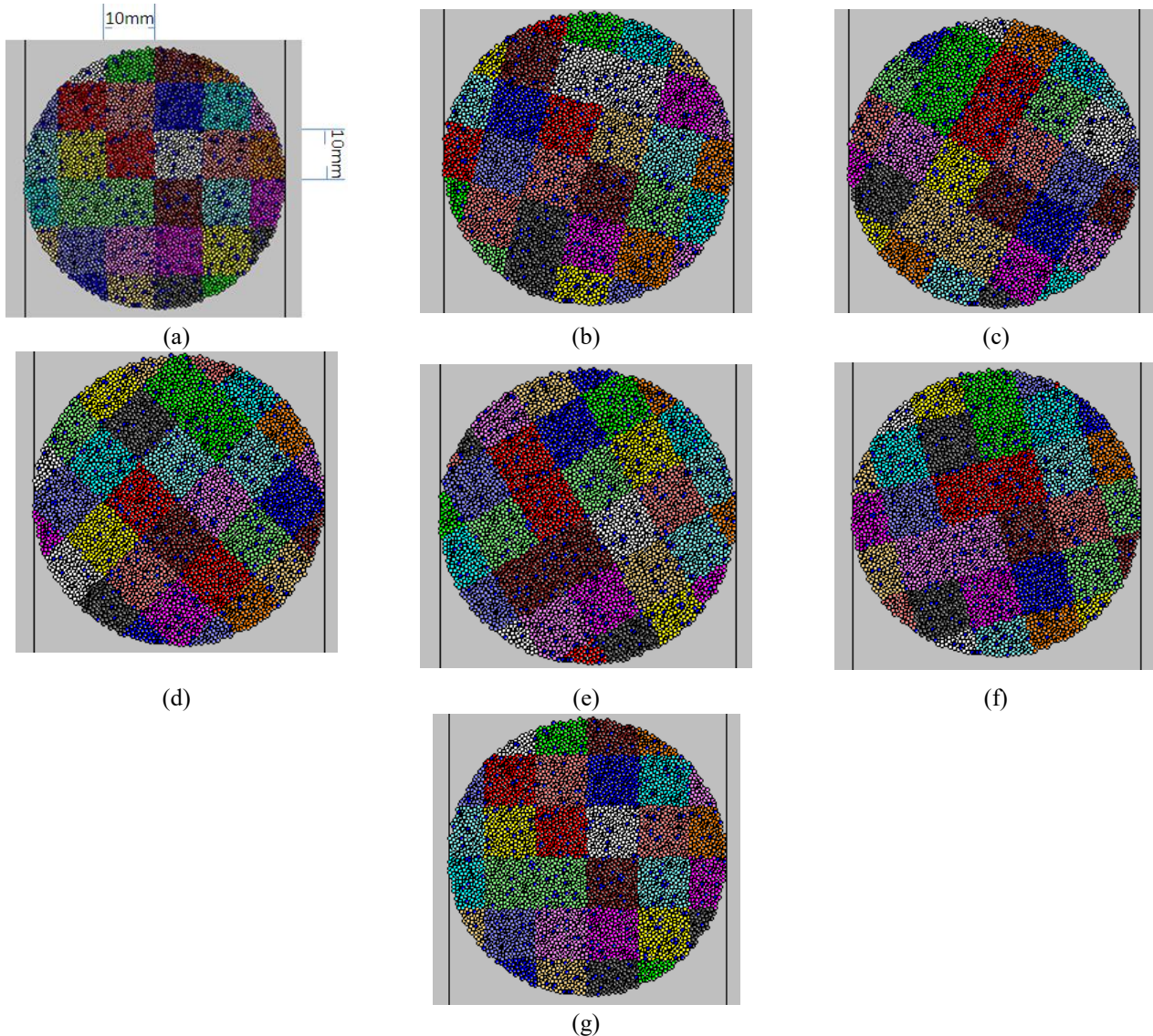


Fig. 4 The models with bedding layers thicknesses of 10 mm and 10 mm; bedding layers angle are (a) 0° - 90° , (b) 15° - 105° , (c) 30° - 120° , (d) 45° - 135° , (e) 60° - 150° , (f) 75° - 165° , (g) 90° - 180°

and too high (Table 3).

3. Results

3.1 The effect of transversely bedding layer on the failure pattern

Figs. 6, 7 and 8 show the effect of transversely bedding layer on the failure pattern of models for bedding thickness of 5 mm/10 mm, 10 mm/10 mm and 20 mm/10 mm; respectively. In each figure the results of interfaces angularities have been shown. Yellow line and black line represent the shear crack and tensile crack, respectively. In all configurations, shear cracks develop between the weaker bedding layers. Shear cracks angel related to normal load change from 0° to 90° with increment of 15° . Numbers of shear cracks are constant by increasing the bedding thickness. It's to be note that in some configuration, tensile cracks develop through the intact area of material model.

There is not any failure in direction of bedding plane interface with higher strength.

3.2 The effect of transversely bedding layer on the Brazilian tensile strength

Fig. 9 shows the effect of transversely bedding layer on the Brazilian tensile strength for bedding thickness of 5 mm/10 mm, 10 mm/10 mm and 20 mm/10 mm; respectively. In this figure the results of interfaces angularities have been shown. The minimum Brazilian strength was occurred when weaker interface angle is between the 30° and 60° . The maximum value occurred in 90° . Also, the Brazilian tensile strength was increased by increasing the layer thickness.

4. Conclusions

In this work, the failure mechanism of transversally

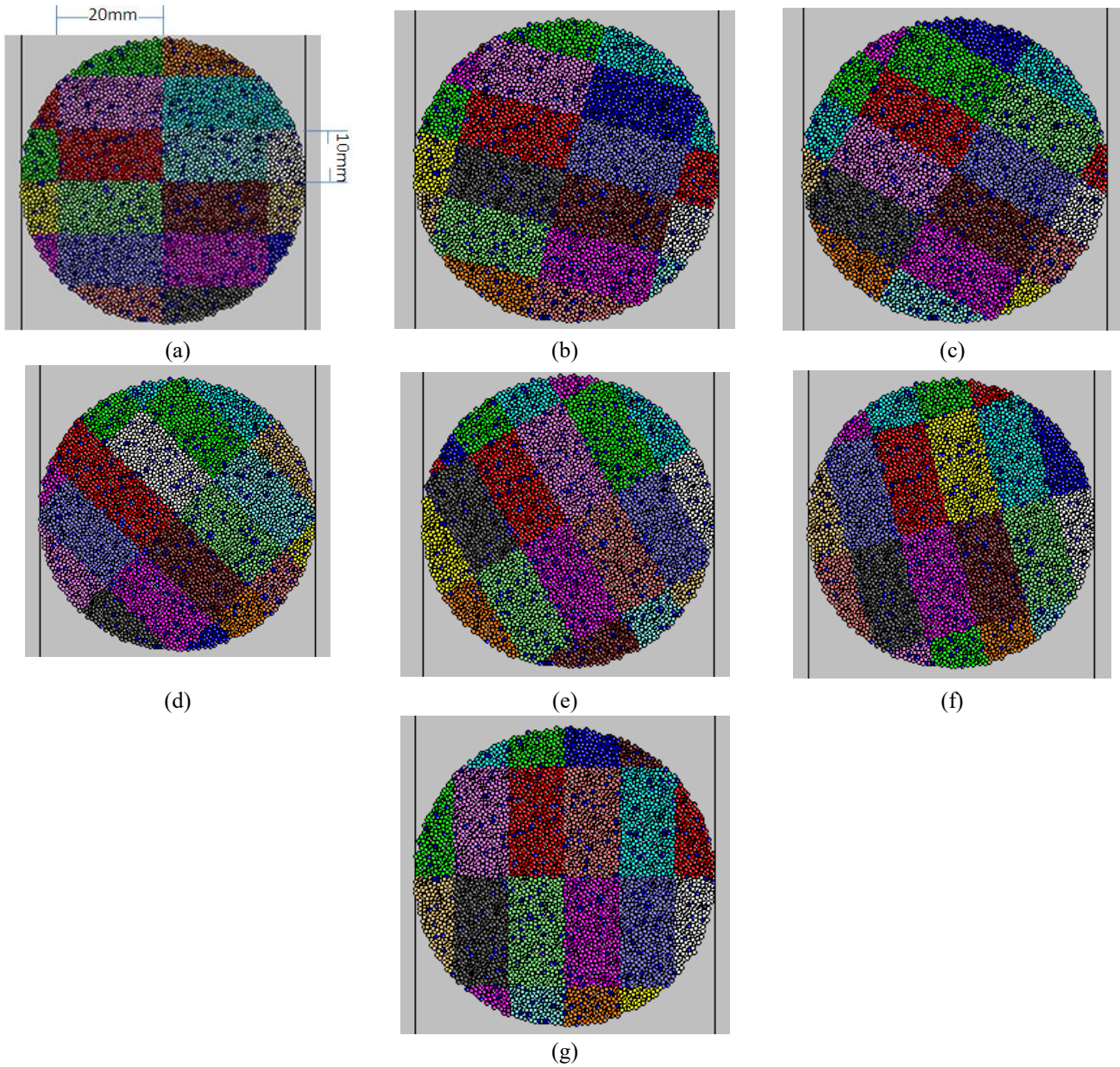


Fig. 5 The models with bedding layers thicknesses of 20 mm and 10 mm; bedding layers angle are (a) 0°-90°, (b) 15°-105°, (c) 30°-120°, (d) 45°-135°, (e) 60°-150°, (f) 75°-165°, (g) 90°-180°

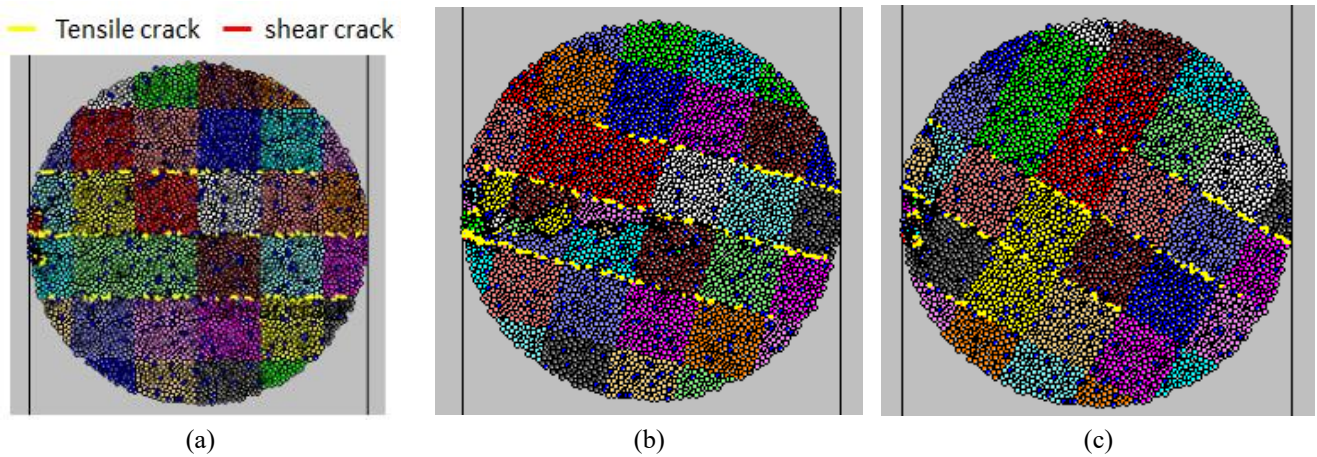


Fig. 6 Failure pattern of the models with bedding layers thicknesses of 10 mm and 10 mm; bedding layers angle are (a) 0°-90°, (b) 15°-105°, (c) 30°-120°, (d) 45°-135°, (e) 60°-150°, (f) 75°-165°, (g) 90°-180°

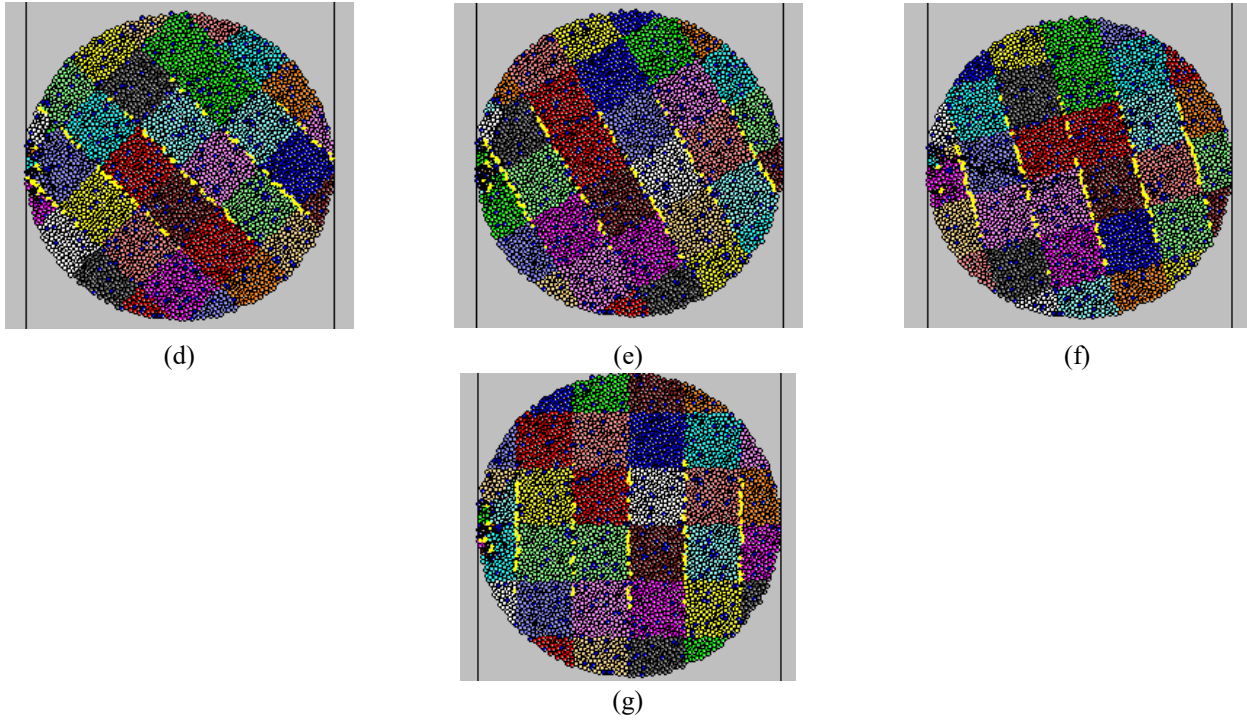


Fig. 6 Continued

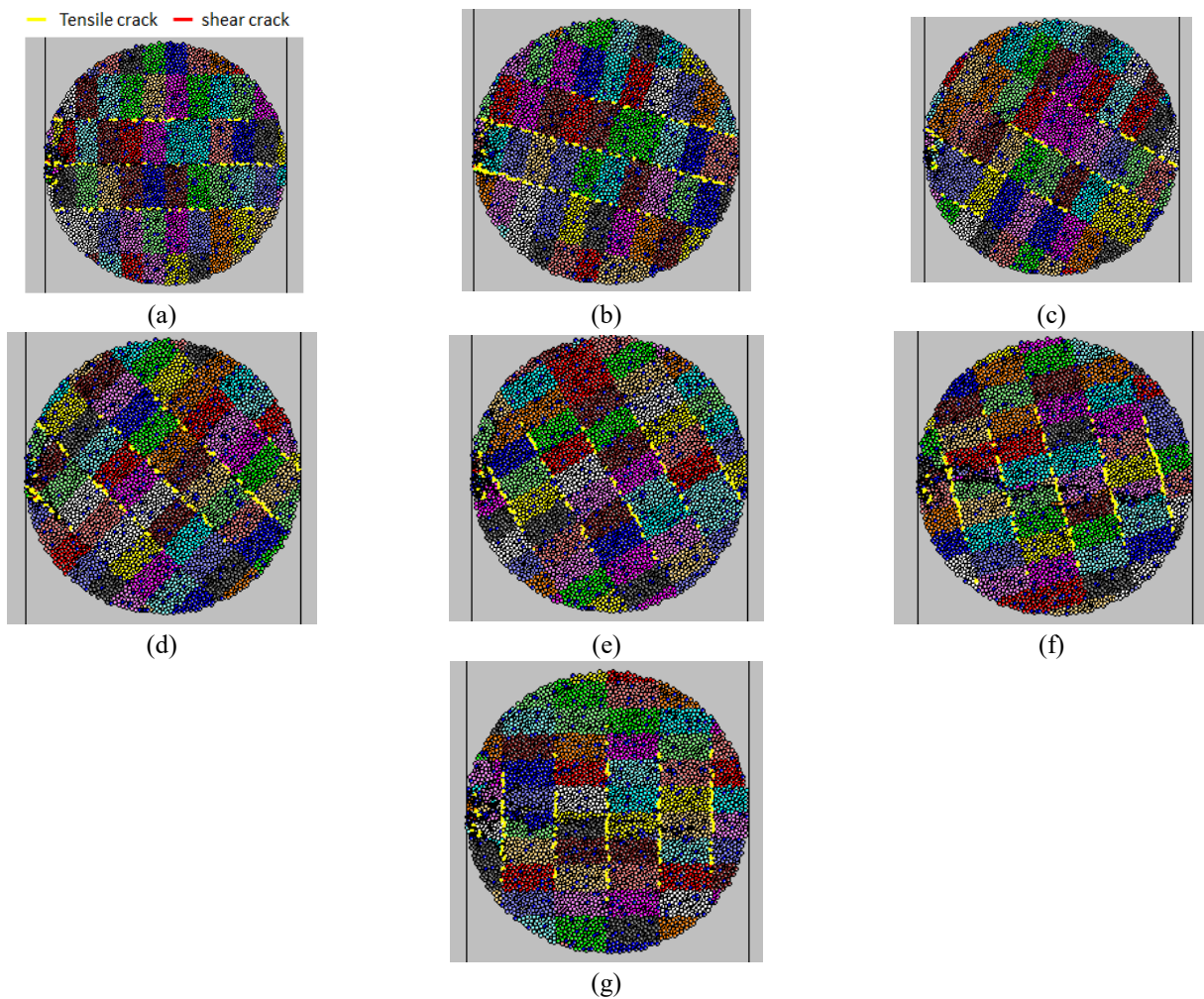


Fig. 7 Failure pattern of the models with bedding layers thicknesses of 5 mm and 10 mm; bedding layers angle are (a) 0° - 90° , (b) 15° - 105° , (c) 30° - 120° , (d) 45° - 135° , (e) 60° - 150° , (f) 75° - 165° , (g) 90° - 180°

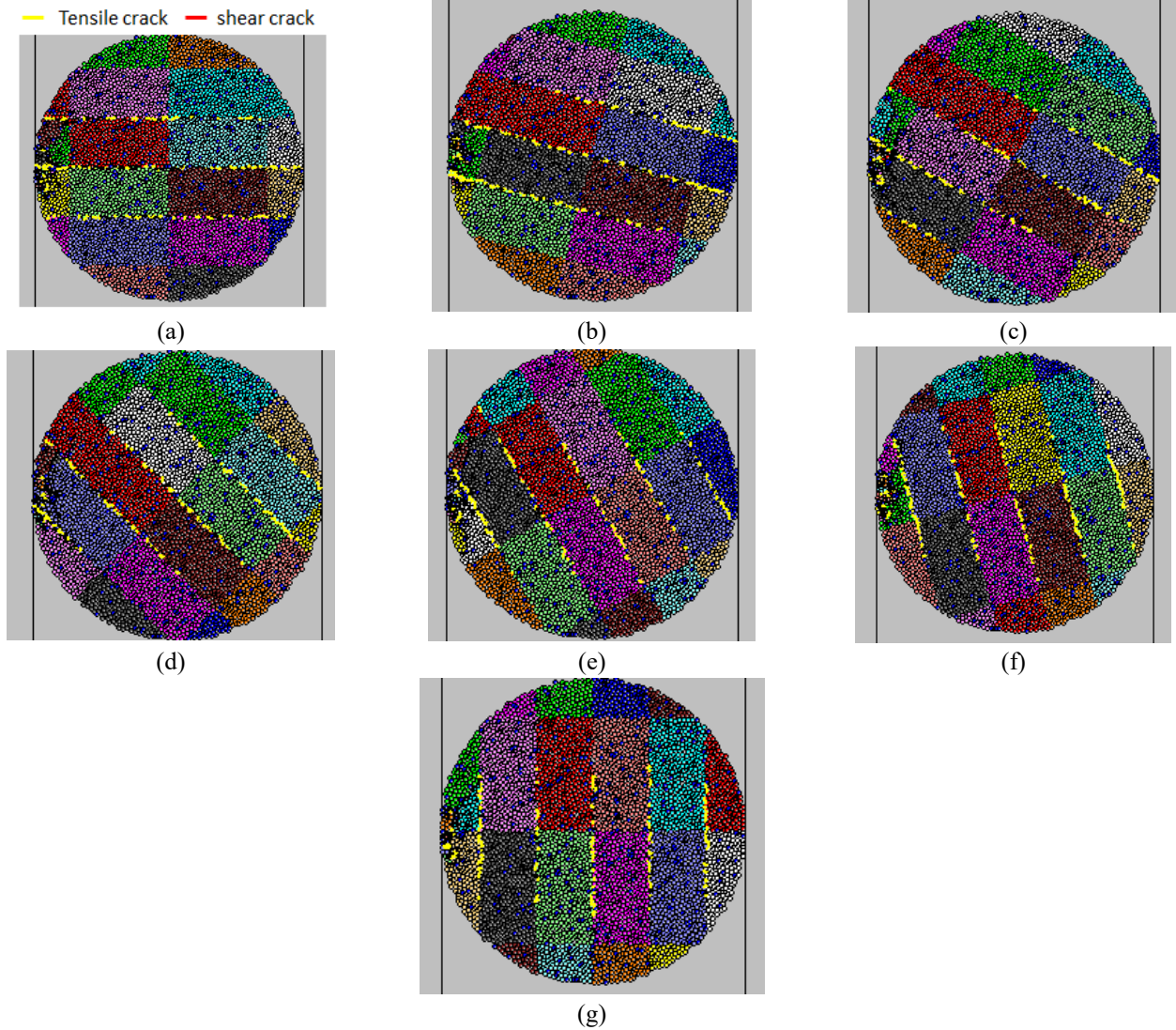


Fig. 8 Failure pattern of the models with bedding layers thicknesses of 20 mm and 10 mm; bedding layers angle are (a) 0°-90°, (b) 15°-105°, (c) 30°-120°, (d) 45°-135°, (e) 60°-150°, (f) 75°-165°, (g) 90°-180°

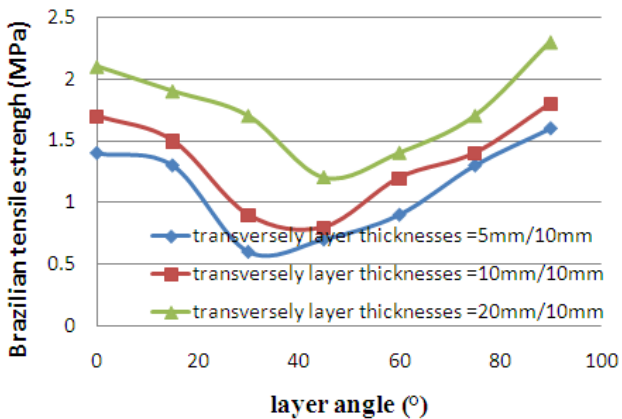


Fig 9 the effect of transversely bedding layer on the Brazilian tensile strength

bedding layers were numerically simulated by using PFC2D. Firstly, numerical model was calibrated by uniaxial, Brazilian and triaxial experimental results to

ensure the conformity of the simulated numerical model's response. Secondly, 21 circular models with diameter of 54 mm were built. Each model contains two transversely bedding layers. The first bedding layer has low mechanical properties, less than mechanical properties of intact material, and second bedding layer has high mechanical properties, more than mechanical properties of intact material. The angle of first bedding layer, with weak mechanical properties, related to loading direction was 0°, 15°, 30°, 45°, 60°, 75° and 90° while the angle of second layer, with high mechanical properties, related to loading direction was 90°, 105°, 120°, 135°, 150°, 160° and 180°. It is to be note that the angle between bedding layer was 90° in all bedding configurations. Also, three different pairs of the thickness was chosen in models; i.e., 5 mm/10 mm, 10 mm/10 mm and 20 mm/10mm. The result shows that in all configurations, shear cracks develop between the weaker bedding layers. Shear cracks angel related to normal load change from 0° to 90° with increment of 15°. Numbers of shear cracks are constant by increasing the bedding thickness. It's to be note that in some configuration, tensile

cracks develop through the intact area of material model. There is not any failure in direction of bedding plane interface with higher strength. The minimum Brazilian strength was occurred when weaker interface angle is between the 30° and 60°. The maximum value occurred in 90°. Also, the Brazilian tensile strength was increased by increasing the layer thickness.

References

- Amadei, B. (1996), "Importance of anisotropy when estimating and measuring in situ stresses in rock", *Int. J. Rock Mech. Min. Sci.*, **33**(3), 293-325.
- Bahaaddini, M., Hagan, P.C., Mitra, R. and Hebblewhite, B.K. (2014), "Scale effect on the shear behaviour of rock joints based on a numerical study", *Eng. Geol.*, **181**, 212-223.
- Bahaaddini, M., Hagan, P.C., Mitra, R. and Hebblewhite, B.K. (2016a), "Numerical study of the mechanical behavior of non-persistent jointed rock masses", *Int. J. Geomech.*, **16**(1), 1-10.
- Bahaaddini, M., Hagan, P.C., Mitra, R. and Khosravi, M.H. (2016b), "Experimental and numerical study of asperity degradation in the direct shear test", *Eng. Geol.*, **204**, 41-52.
- Cho, J.W., Kim, H., Jeon, S.W. and Min, K.B. (2012), "Deformation and strength anisotropy of Asan gneiss, Boryeong shale, and Yeoncheon schist", *Int. J. Rock Mech. Min. Sci.*, **50**, 158-169.
- Dan, D.Q. and Konietzky, H. (2014), "Numerical simulations and interpretations of Brazilian tensile tests on transversely isotropic rocks", *Int. J. Rock Mech. Min. Sci.*, **71**, 53-63.
- Dan, D.Q., Konietzky, H. and Herbst, M. (2013), "Brazilian tensile strength tests on some anisotropic rocks", *Int. J. Rock Mech. Min. Sci.*, **58**, 1-7.
- Duan, K. and Kwok, C.Y. (2015), "Discrete element modeling of anisotropic rock under Brazilian test conditions", *Int. J. Rock Mech. Min. Sci.*, **78**, 46-56.
- Fan, Y., Zhu, Z., Kang, J. and Fu, Y. (2016), "The mutual effects between two unequal collinear cracks under compression", *Math. Mech. Sol.*, **22**(5), 1205-1218.
- Fortsakis, P., Nikas, K., Marinou, V. and Marinou, P. (2012), "Anisotropic behaviour of stratified rock masses in tunneling", *Eng. Geol.*, **141**, 74-83.
- Gerges, N., Issa, C. and Fawaz, S. (2015), "Effect of construction joints on the splitting tensile strength of concrete", *Case Stud. Constr. Mater.*, **3**, 83-91.
- Gholami, R. and Rasouli, V. (2014), "Mechanical and elastic properties of transversely isotropic slate", *Rock Mech. Rock Eng.*, **47**(5), 1763-1773.
- Haeri, H. (2015), "Influence of the inclined edge notches on the shear-fracture behavior in edge-notched beam specimens", *Comput. Concrete*, **16**(4), 605-623.
- Haeri, H. (2015), "Simulating the crack propagation mechanism of pre-cracked concrete specimens under shear loading conditions", *Strength Mater.*, **47**(4), 618-632.
- Haeri, H. and Sarfarazi, V. (2016), "The effect of micro pore on the characteristics of crack tip plastic zone in concrete", *Comput. Concrete*, **17**(1), 107-112.
- Haeri, H. and Sarfarazi, V. (2016), "The effect of non-persistent joints on sliding direction of rock slopes", *Comput. Concrete*, **17**(6), 723-737.
- Haeri, H., Khaloo, A. and Marji, M.F. (2014), "A coupled experimental and numerical simulation of rock slope joints behavior", *Arab. J. Geosci.*, **8**(9), 7729-7308.
- Haeri, H., Khaloo, A. and Marji, M.F. (2015a), "Experimental and numerical simulation of the microcrack coalescence mechanism in rock-like materials", *Strength Mater.*, **47**(5), 740-754.
- Haeri, H., Khaloo, A. and Marji, M.F. (2015b), "Fracture analyses of different pre-holed concrete specimens under compression", *Acta Mech. Sin.*, **31**(6), 855-870.
- Haeri, H., Khaloo, A. and Marji, M.F. (2016a), "Fracture analyses of different preholed concrete specimens under compression", *Acta Mech. Sin.*, **31**(6), 855-870.
- Haeri, H., Sarfarazi, V. and Hedayat, A. (2016), "Suggesting a new testing device for determination of tensile strength of concrete", *Struct. Eng. Mech.*, **60**(6), 939-952.
- Haeri, H., Sarfarazi, V. and Lazemi, H.A. (2016b), "Experimental study of shear behavior of planar non-persistent joint", *Comput. Concrete*, **17**(5), 639-653.
- Haeri, H., Shahriar, K., Marji, M.F. and Moarefvand, P. (2013), "Modeling the propagation mechanism of two random micro cracks in rock samples under uniform tensile loading", *Proceedings of the 13th International Conference on Fracture*, Beijing, China, June.
- Jia, P. and Tang, C.A. (2008), "Numerical study on failure mechanism of tunnel in jointed rock mass", *Tunn. Undergr. Space Technol.*, **23**(5), 500-507.
- Jia, P. and Tang, C.A. (2008), "Numerical study on failure mechanism of tunnel in jointed rock mass", *Tunn. Undergr. Space Technol.*, **23**(5), 500-507.
- Jiang, Y., Tanabashi, Y., Li, B. and Xiao, J. (2006), "Influence of geometrical distribution of rock joints on deformational behavior of underground opening", *Tunn. Undergr. Space Technol.*, **21**(5), 485-491.
- Johansson, F. (2016), "Influence of scale and matedness on the peak shear strength of fresh, unweathered rock joints", *Int. J. Rock Mech. Min. Sci.*, **82**, 36-47.
- Khanlari, G., Rafiei, B. and Abdilor, Y. (2015), "An experimental investigation of the Brazilian tensile strength and failure patterns of laminated sandstones", *Rock Mech. Rock Eng.*, **48**(2), 843-852.
- Khosravi, A., Simon, R. and Rivard, P. (2017), "The shape effect on the morphology of the fracture surface induced by the Brazilian test", *Int. J. Rock Mech. Min. Sci.*, **93**, 201-209.
- Kim, J. and Taha, M.R. (2014), "Experimental and numerical evaluation of direct tension test for cylindrical concrete specimens", *Adv. Civil Eng.*, 1-8.
- Lancaster, I.M. and Khalid, H.A. and Kougioumtzoglou, I.A. (2013), "Extended FEM modelling of crack propagation using the semi-circular bending test", *Constr. Build. Mater.*, **48**, 270-277.
- Lazear, G.D. (2009), "Fractures, convection and under pressure: Hydrogeology on the Southern margin of the Piceance basin, west-central Colorado, USA", *Hydrogeol. J.*, **17**(3), 641-664.
- Li, L.C., Xia, Y.J., Huang, B., Zhang, L.Y., Li, M. and Li, A.S. (2016), "The behaviour of fracture growth in sedimentary rocks: A numerical study based on hydraulic fracturing processes", *Energies*, **9**(3), 169-197.
- Li, S., Wang, H., Li, Y., Li, Q., Zhang, B. and Zhu, H. (2016), "A new mini-grating absolute displacement measuring system for static and dynamic geomechanical model tests", *Measure.*, **82**, 421-431.
- Li, X.L. (2013), "Timodaz: A successful international cooperation project to investigate the thermal impact on the EDZ around a radioactive waste disposal in clay host rocks", *J. Rock Mech. Geotech. Eng.*, **5**(3), 231-242.
- Lisjak, A., Garitte, B., Grasselli, G., Müller, H.R. and Vietor, T. (2015), "The excavation of a circular tunnel in a bedded argillaceous rock (opaline clay): Short-term rock mass response and FDEM numerical analysis", *Tunn. Undergr. Space Technol.*, **45**, 227-248.
- Liu, K.D., Liu, Q.S., Zhu, Y.G. and Liu, B. (2013), "Experimental study of coal considering directivity effect of bedding plane under Brazilian splitting and uniaxial compression", *Chin. J.*

- Rock Mech. Eng.*, **32**(2), 308-316.
- Liu, X., Nie, Z., Wu, S. and Wang, C. (2015), "Self-monitoring application of conductive asphalt concrete under indirect tensile deformation, case studies in construction materials", **3**, 70-77.
- Ma, T., Wu, B., Fu, J., Zhang, Q. and Chen, P. (2017b), "Fracture pressure prediction for layered formations with anisotropic rock strengths", *J. Nat. Gas Sci. Eng.*, **38**, 485-503.
- Ma, T., Zhang, Q.B., Chen, P., Yang, C. and Zhao, J. (2017a), "Fracture pressure model for inclined wells in layered formations with anisotropic rock strengths", *J. Petrol. Sci. Eng.*, **149**, 393-408.
- Min, K.B. and Jing, L.R. (2003), "Numerical determination of the equivalent elastic compliance tensor for fractured rock masses using the distinct element method", *Int. J. Rock Mech. Min. Sci.*, **40**(6), 795-816.
- Mobasher, B., Bakhshi, M. and Barsby, C. (2014), "Backcalculation of residual tensile strength of regular and high performance fibre reinforced concrete from flexural tests", *Constr. Build. Mater.*, **70**, 243-253.
- Noel, M. and Soudki, K. (2014), "Estimation of the crack width and deformation of FRP-reinforced concrete flexural members with and without transverse shear reinforcement", *Eng. Struct.*, **59**, 393-398.
- Oliveira, H.L. and Leonel, E.D. (2014), "An alternative BEM formulation, based on dipoles of stresses and tangent operator technique, applied to cohesive crack growth modeling", *Eng. Anal. Bound. Elem.*, **41**, 74-82.
- Sardemir, M. (2016), "Empirical modeling of flexural and splitting tensile strengths of concrete containing fly ash by GEP", *Comput. Concrete*, **17**(4), 489-498.
- Sarfarazi, V., Faridi, H.R., Haeri, H. and Schubert, W. (2016c), "A new approach for measurement of anisotropic tensile strength of concrete", *Adv. Concrete Constr.*, **3**(4), 269-284.
- Sarfarazi, V., Haeri, H. and Bagher Shemirani, A. (2017a), "Direct and indirect methods for determination of mode I fracture toughness using PFC2D", *Comput. Concrete*, **20**(1), 39-47.
- Sarfarazi, V., Haeri, H., Bagher Shemirani, A. and Zhu, Z. (2017b), "The effect of compression load and rock bridge geometry on the shear mechanism of weak plane", *Geomech. Eng.*, **13**(3), 57-63.
- Sarfarazi, V., Haeri, H., Bagher Shemirani, A., Hedayat, A. and Hosseini, S. (2017c), "Investigation of ratio of TBM disc spacing to penetration depth in rocks with different tensile strengths using PFC2D", *Comput. Concrete*, **20**(4), 429-437.
- Seingre, G. (2005), *Tunnel de Base du Lötschberg-Bil an de L'excavation aux Tunneliers*, In: Arnould, M., Ledru, P. (Eds.), GEOLINE 2005, BRGM editions. Lyon, France, May.
- Shuraim, A.B., Aslam, F., Hussain, R. and Alhozaimy, A. (2016), "Analysis of punching shear in high strength RC panels-experiments, comparison with codes and FEM results", *Comput. Concrete*, **17**(6), 739-760.
- Silva, R.V., Brito, J. and Dhir, R.K. (2015), "Tensile strength behaviour of recycled aggregate concrete", *Constr. Build. Mater.*, **83**, 108-118.
- Tavallali, A. and Vervoort, A. (2010), "Effect of layer orientation on the failure of layered sandstone under Brazilian test conditions", *Int. J. Rock Mech. Min. Sci.*, **47**(2), 313-322.
- Tiang, Y., Shi, S., Jia, K. and Hu, S. "Mechanical and dynamic properties of high strength concrete modified with lightweight aggregates presaturated polymer emulsion", *Constr. Build. Mater.*, **93**, 1151-1156.
- Vervoort, A., Min, K.B., Konietzky, H., Cho, J.W., Debecker, B., Dinh, Q.D., Frühwirth, T. and Tavallali, A. (2014), "Failure of transversely isotropic rock under Brazilian test conditions", *Int. J. Rock Mech. Min. Sci.*, **70**, 343-352.
- Wan Ibrahim, M.H., Hamzah, A.F., Jamaluddin, N., Ramadhansyah, P.J. and Fadzil, A.M. (2015), "Split tensile strength on self-compacting concrete containing coal bottom ash", *Proc.-Soc. Behav. Sci.*, **198**, 2280-2289.
- Wang, J., Xie, L.Z., Xie, H.P., Ren, L., He, B., Li, C.B., Yang, Z.P. and Gao, C. (2016a), "Effect of layer orientation on acoustic emission characteristics of anisotropic shale in Brazilian tests", *J. Nat. Gas Sci. Eng.*, **36**, 1120-1129.
- Wang, P.T., Ren, F.H., Miao, S.J., Cai, M.F. and Yang, T.H. (2017), "Evaluation of the anisotropy and directionality of a jointed rock mass under numerical direct shear tests", *Eng. Geol.*, **225**, 29-41.
- Wang, P.T., Yang, T.H., Xu, T., Cai, M.F. and Li, C.H. (2016b), "Numerical analysis on scale effect of elasticity, strength and failure patterns of jointed rock masses", *Geosci. J.*, **20**(4), 539-549.
- Wang, S.Y., Sloan, S.W., Tang, C.A. and Zhu, W.C. (2012), "Numerical simulation of the failure mechanism of circular tunnels in transversely isotropic rock masses", *Tunn. Undergr. Space Technol.*, **32**, 231-244.
- Wang, T., Xu, D., Elsworth, D. and Zhou, W. (2016c), "Distinct element modeling of strength variation in jointed rock masses under uniaxial compression", *Geomech. Geophys. Geo-Eng. Geo-Res.*, **2**(1), 11-24.
- Wang, Y.T., Zhou, X.P. and Shou, Y.D. (2017), "The modeling of crack propagation and coalescence in rocks under uniaxial compression using the novel conjugated bond-based peridynamics", *Int. J. Mech. Sci.*, **128**, 614-643.
- Wasantha, P.L.P., Ranjith, P.G., Zhang, Q.B. and Xu, T. (2015), "Do joint geometrical properties influence the fracturing behaviour of jointed rock? An investigation through joint orientation", *J. Geomech. Geophys. Geol. Energy Geol. Res.*, **1**(1-2), 3-14.
- Wu, W., Wang, G.B. and Mao, H.J. (2010), "Investigation of porosity effect on mechanical strength characteristics of dolostone", *Rock Soil Mech.*, **31**(12), 3709-3714.
- Xia, K., Yao, W. and Wu, B. (2017), "Dynamic rock tensile strengths of Laurentian granite: Experimental observation and micromechanical model", *J. Rock Mech. Geotech. Eng.*, **9**(1), 116-124.
- Xu, T., Ranjith, P.G., Wasantha, P.L.P., Zhao, J., Tang, C.A. and Zhu, W.C. (2013), "Influence of the geometry of partially-spanning joints on mechanical properties of rock in uniaxial compression", *Eng. Geol.*, **167**, 134-147.
- Yang, T., Liu, H.Y. and Tang, C.A. (2017), "Scale effect in macroscopic permeability of jointed rock mass using a coupled stress-damage-flow method", *Eng. Geol.*, **228**, 121-136.
- Yang, T.H., Wang, P.T., Xu, T., Yu, Q.L., Zhang, P.H., Shi, W.H. and Hu, G.J. (2015), "Anisotropic characteristics of fractured rock mass and a case study in Shirengou metal mine in China", *Tunn. Undergr. Space Technol.*, **48**, 129-139.
- Yu, L., Weetjens, E., Sillen, X., Victor, T., Li, X., Delage, P., Labiouse, V. and Charlier, R. (2014), "Consequences of the thermal transient on the evolution of the damaged zone around a repository for heat-emitting high-level radioactive waste in a clay formation: A performance assessment perspective", *Rock Mech. Rock Eng.*, **47**(1), 3-19.
- Yuan, R. and Shen, B. (2017), "Numerical modelling of the contact condition of a Brazilian disk test and its influence on the tensile strength of rock", *Int. J. Rock Mech. Min. Sci.*, **93**, 54-65.
- Zhang, S.W., Shou, K.J., Xian, X.F., Zhou, J.P. and Liu, G.J. (2018), "Fractal characteristics and acoustic emission of anisotropic shale in Brazilian tests", *Tunn. Undergr. Space Technol.*, **71**, 298-308.
- Zhou, J.R., Wei, J., Yang, T.H., Zhu, W.C., Li, L.C. and Zhang, P.H. (2018), "Damage analysis of rock mass coupling joints, water and microseismicity", *Tunn. Undergr. Space Technol.*, **71**, 366-381.
- Zhou, X.P. and Bi, J. (2018), "Numerical simulation of thermal

- cracking in rocks based on general particle dynamics”, *J. Eng. Mech.*, **144**(1), 04017156.
- Zhou, X.P. and Wang, Y.T. (2016), “Numerical simulation of crack propagation and coalescence in pre-cracked rock-like Brazilian disks using the non-ordinary state-based peridynamics”, *Int. J. Rock Mech. Min. Sci.*, **89**, 235-249.
- Zhou, X.P. and Yang, H.Q. (2012), “Multiscale numerical modeling of propagation and coalescence of multiple cracks in rock masses”, *Int. J. Rock Mech. Min. Sci.*, **55**, 15-27.

CC